

This document contains a post-print version of the paper

Model-Predictive Control of Servo-Pump Driven Injection Molding Machines

authored by **C. Froehlich, W. Kemmetmüller, and A. Kugi**
and published in *IEEE Transactions on Control Systems Technology*.

The content of this post-print version is identical to the published paper but without the publisher's final layout or copy editing. Please, scroll down for the article.

Cite this article as:

C. Froehlich, W. Kemmetmüller, and A. Kugi, "Model-predictive control of servo-pump driven injection molding machines," *IEEE Transactions on Control Systems Technology*, vol. 28, no. 5, pp. 1665–1680, 2020, ISSN: 1063-6536. DOI: [10.1109/TCST.2019.2918993](https://doi.org/10.1109/TCST.2019.2918993)

BibTex entry:

```
@Article{acinpaper,  
  author = {Froehlich, C. and Kemmetmüller, W. and Kugi, A.},  
  journal = {IEEE Transactions on Control Systems Technology},  
  title = {Model-Predictive Control of Servo-Pump Driven Injection Molding Machines},  
  year = {2020},  
  issn = {1063-6536},  
  number = {5},  
  pages = {1665-1680},  
  volume = {28},  
  doi = {10.1109/TCST.2019.2918993},  
  timestamp = {2020-11-05},  
}
```

Link to original paper:

<http://dx.doi.org/10.1109/TCST.2019.2918993>

Read more ACIN papers or get this document:

<http://www.acin.tuwien.ac.at/literature>

Contact:

Automation and Control Institute (ACIN)
TU Wien
Gusshausstrasse 27-29/E376
1040 Vienna, Austria

Internet: www.acin.tuwien.ac.at
E-mail: office@acin.tuwien.ac.at
Phone: +43 1 58801 37601
Fax: +43 1 58801 37699

Copyright notice:

© 2020 IEEE. Personal use of this material is permitted. Permission from IEEE must be obtained for all other uses, in any current or future media, including reprinting/republishing this material for advertising or promotional purposes, creating new collective works, for resale or redistribution to servers or lists, or reuse of any copyrighted component of this work in other works.

Model-predictive control of servo-pump driven injection molding machines

Christoph Froehlich, *Member, IEEE*, Wolfgang Kemmetmüller, *Member, IEEE*, and Andreas Kugi, *Member, IEEE*

Abstract—A high-dynamic and accurate control of the process variables within their admissible limits is essential to meet a high product quality in injection molding processes. Conventional control concepts of hydraulic injection molding machines typically employ servo-valves or variable displacement pumps as actuators. Nowadays, servo-motor driven pumps are frequently used due to their higher energy efficiency. These systems, however, exhibit a slower actuator dynamics and thus demand for more advanced control concepts. This paper proposes a novel control concept for this type of injection molding machines consisting of a Lyapunov-based load volume flow estimator and a model-predictive controller based on a Riccati recursion. The control concept systematically accounts for the system constraints and features a high performance for the filling and packing phase without knowledge of the mold geometry or information from previous injection cycles. A thorough comparison of the proposed control strategy with the industrial state-of-the-art controller is made by injection and melt cushion experiments on an industrial injection molding machine. Finally, also the robustness of the proposed control concept with respect to model uncertainties is shown.

Index Terms—Nonlinear Control Systems, Injection Molding, Process Control, Model-Predictive Control

I. INTRODUCTION

INJECTION molding is a widely applied manufacturing process for shaping plastic products of various sizes and forms. Fig. 1 gives an overview of the considered injection unit. In contrast to the classical setup of hydraulic injection units, where the servo-valve is used for controlling the injection process, the servo-driven internal gear pump serves as the actuator for the controller design. This makes the overall system more energy efficient, but at the cost of a slower actuator dynamics and thus a more challenging controller design. The cyclic production process consists of the following phases: First, the reciprocating screw is moved towards the nozzle and the molten polymer is injected from the antechamber through the nozzle into the mold (filling phase). Then a high pressure is applied in the packing phase to completely fill the mold and get the desired mechanical properties of the product after the cooling phase. As soon as the melt delivery channel is frozen (in cold runner molds) or actively closed (in hot runner molds), i. e., no more polymer can flow into the mold, the screw is rotated by the plastication drive. This feeds cold granulate from the hopper towards the antechamber. Inside the heated barrel the polymer is molten and homogeneously mixed. In the end of the cycle, the mold is opened and the finished part

The authors are with the Automation and Control Institute, TU Wien, 1040 Vienna, Austria (e-mail: froehlich@acin.tuwien.ac.at; kemmetmueller@acin.tuwien.ac.at; kugi@acin.tuwien.ac.at).

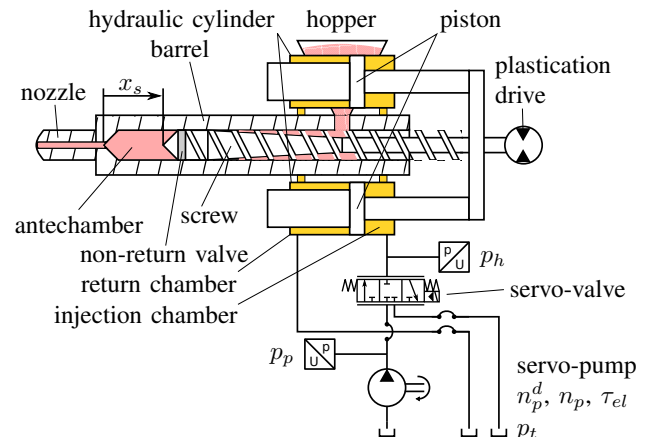


Fig. 1. Overview of the hydraulic injection unit [1].

is ejected. For a detailed description of the injection molding process see, e. g., [2], [3].

The control of the injection molding process is a challenging task, mainly due to the nonlinear system dynamics resulting from the properties of the polymer, the complex geometries of the molds, and the nonlinear actuator dynamics. An overview of different existing control approaches for the injection molding process can be found, e. g., in [2], [4]. An accurate control of the process variables (as, e. g., the mass flow into the mold, the pressures in the mold, etc.), especially during the filling and packing phase, is crucial for the final product quality. However, a direct measurement of these process variables is mostly not possible. Instead, measurable machine variables (as, e. g., the injection speed or injection pressure) are used for the control task. For the considered type of injection molding machines, typically the injection speed is controlled in the filling phase, while the injection pressure is controlled in the packing phase. The transfer point between these two control tasks can be chosen by the operator, either as a function of the screw position, the injection time, or the injection pressure.

Furthermore, a practically feasible control strategy has to take into account the following conditions: (i) The control performance should be identical in every cycle. In particular, a high control performance has to be ensured already from the first cycle on. Thus, despite the repetitive nature of injection molding, in this paper the control concept should not rely on information from previous cycles. (ii) Since the exact mold geometry is often not available for the controller, this information should not be used in the control design. Moreover, the control performance should be identical for

different molds without the need for separately adjusting the control parameters. (iii) The desired trajectories given by the operator typically do not comply with the physical constraints of the system. For the considered hydraulic injection unit, the essential constraints are the maximum injection pressure, the maximum rotational speed and torque of the servo-drive, and the maximum slew-rate of the hydraulic pump speed. (iv) The injection process is characterized by a fast dynamics. In particular, very fast pressure rises can occur when the mold is completely filled [2], [3]. To protect the mold and the injection unit, a suitable control strategy has to accurately control the injection pressure and has to ensure that it always stays within the admissible system limits.

A. Existing Solutions

To master these challenges, extensive research has been conducted over the last decades. Agrawal et al. [4] gave an overview of the control concepts up to the late 1980s, where conventional PI/PID controllers were commonly used [5], [6]. Up to now these controllers are still state of the art in industry. These linear control concepts have been extended and improved by various authors. Pandelidis and Agrawal [7] proposed an optimal state controller. Dong and Tseng [8] discussed the application of self-tuning regulators for injection molding machines. Smud et al. [9] developed simple predictive controllers based on input-output responses. Zhang and Gao [10] proposed an optimal state controller based on input-output process data, capable of handling partial actuator failure. Predictive controllers based on input-output data like dynamic matrix controllers [11], [12], general predictive controllers [13], [14], extended predictive controllers to systematically derive the tuning parameters [15], or multi-model predictive controllers [16], [17] show promising improvements compared to conventional PI/PID controllers. Although these controllers rely on a calibration of the tuning parameters or extensive measurement campaigns for collecting input-output data, they are not able to show the same high performance for the whole operating range and different molds.

This issue has been addressed by the development of model-based nonlinear controllers. Yang [18] applied an adaptive backstepping method with estimating two unknown process parameters. Tan et al. [19] proposed a sliding mode controller. Daxberger et al. [20] developed nonlinear control laws together with a Lyapunov estimator for the unknown mold behavior and Lindert et al. [21] used a flatness-based control approach for the ram position. All these methods have in common that they are based on a mathematical model of the system. However, the limiting constraints were not systematically considered in the controller design. Furthermore, no measurement results were presented, leaving open questions of their practical applicability and robustness with respect to parameter variations, model inaccuracies and sensor noise.

As an alternative, several model-free control approaches have been proposed. One example are fuzzy logic rule-based controllers. The drawback of this type of controllers is that a systematic way of choosing the membership functions is quite difficult [22], [23]. Lin and Lian [24] propose to utilize training

data in a neural network to learn these membership functions. Neural networks were also investigated to train a feedforward control in combination with linear feedback controllers [25], [26]. Because the learning phase of these concepts relies on the availability of a sufficient amount of high quality training data, these concepts require a long calibration phase for every type of machine or product, which limits their practical feasibility.

In contrast to the previously mentioned control strategies, iterative learning concepts exploit the repetitive nature of the injection molding process [23], [27], [28], [29], [30], [31], [32], [33]. These concepts, however, exhibit a poor performance in the first cycles and thus do not meet the requirements of having a high performance already from the first cycle on.

Most of these given publications solve the control problem only for one phase of the process, either the filling or the packing phase. In order to cover both phases without provoking discontinuities a seamless transition strategy or a common controller for both phases is required. Havlicsek and Alleyne [27], [30] solved this problem with independent controllers and a bumpless transfer scheme at switchover. Huang and Lee [34] trained two independent neural networks for both phases reducing the overshoot after switchover. Lin and Lian [24] developed two independent fuzzy logic rule-based controllers for both phases. Dorner et al. [33] solved the switchover by adapting the cost function at the switchover point with the same optimal iterative learning controller for both phases.

As already discussed before, several constraints have to be considered for the injection molding process. In the literature, only few publications address this issue. One possible method is model-predictive control, which allows to systematically account for these limits. Peng et al. [35] used a neural network solving the underlying optimal control problem. Reiter et al. [36] formulated a model-predictive controller and conducted experiments on a prototype machine. The achieved sampling time of 8 ms is, however, too slow for the rapid injection cycles with very fast dynamic response considered in this paper. Cao et al. [32] proposed a two-time-dimensional model-predictive controller for the weld line position, combining a conventional model-predictive controller with an iterative learning control. Therefore, they use a simplified linear actuator model together with a model for the mold, where the cross-sectional area along the flow path has to be known in advance. Due to these assumptions and the different control task these results are not directly applicable to the control problem addressed in this paper.

Modern hydraulic injection units are often servo-pump driven to reduce the demand of energy and hence the operating costs. The requirements for the controllers significantly increase due to the slower dynamics of the servo-pump compared to the classical setup where the servo-valve serves as actuator for the controller design. For example, filling the mold close to the pressure limit or reacting on the fast pressure overshoot after the complete filling is more challenging with this slower actuator dynamics. The control of this type of actuator has been topic of recent research: Wang et al. [23] proposed a fuzzy PI control for the packing pressure, with the already discussed drawback of shaping the membership functions.

Peng et al. [35] presented a model-predictive controller for the injection speed under some simplifications, e. g., a constant volume flow into the mold was assumed. Furthermore, no proof of real-time capability was given.

B. Objective and Structure of the Paper

Based on the literature review, the following open issues are identified: (i) A control strategy is missing which systematically includes both the filling and the packing phase. (ii) Control strategies tailored to servo-pump driven injection molding machines are required. (iii) The maximum performance of the actuator has to be utilized while still meeting the essential constraints of the system. (iv) The control algorithm must be executable in real time on an industrial automation platform. The present paper addresses these open issues and proposes a real-time capable control strategy meeting the given requirements.

The paper is structured as follows: The mathematical model, which serves as a basis for the controller design, is presented in Sec. II. Sec. III is concerned with the derivation of the control strategy, which consists of an estimator for the unknown polymer flow into the mold and a nonlinear model-predictive controller. The control strategy is finally validated by means of simulations and measurements in Sec. IV. The last section, Sec. V, contains some conclusions.

II. MATHEMATICAL MODEL

The mathematical model serves as a basis for the design of a real-time capable model-based control strategy. This model has to be sufficiently accurate and should cover the essential nonlinearities and the dominating dynamics while still being computationally efficient. Thus, starting from a detailed mathematical model described by the authors in [1], a (simplified) model tailored to the needs of the controller and estimator design is derived in this section.

The motion of the screw (position x_s , velocity $v_s = \dot{x}_s$) is described by

$$\frac{d}{dt}x_s = v_s \quad (1a)$$

$$\frac{d}{dt}v_s = \frac{1}{m_s}(A_{ac}(p_{ac} - p_0) - 2A_{ci}(p_h - p_0) - F_{fr}), \quad (1b)$$

where m_s is the overall mass of the screw and the connected components, $A_{ac} = D_s^2\pi/4$ and A_{ci} are the effective areas of the antechamber (filled with polymer; screw diameter D_s) and the injection side of the cylinder. Moreover, p_0 is the constant ambient pressure, p_h is the cylinder pressure, and the pressure of the polymer in the antechamber is denoted by p_{ac} . The friction force F_{fr} summarizes the friction in the hydraulic cylinder and between the screw and the barrel, cf. [1].

The pressure p_{ac} of the polymer in the antechamber results from the balance of mass in the form [1]

$$\frac{d}{dt}p_{ac} = \frac{\beta_{ac}}{x_0 + x_s + r_s(p_{ac} + \beta_{ac})} \left(-v_s - \frac{q_{no}}{A_{ac}} \right), \quad (2)$$

where r_s accounts for the stiffness of the screw and x_0A_{ac} is the remaining dead volume at $x_s = 0$. The bulk modulus

β_{ac} of the polymer is typically a nonlinear function of the pressure p_{ac} and can be approximated for instance by a Tait model [37]. In the operating range of the machine and for constant temperature, the simpler approximation $\beta_{ac} = \beta_0 + \beta_1 p_{ac} + \beta_2 p_{ac}^2$ with constant parameters β_0, β_1 , and β_2 yields a high accuracy and will therefore be utilized in the following.

The volume flow q_{no} into the mold is described by the power-law model

$$q_{no} = c_{no}(p_{ac} - p_0)^{\frac{1}{n}}, \quad (3)$$

with the polymer flow behavior index n and the time-dependent flow conductance c_{no} , see [1] for a detailed discussion. If the pressure drop in the piping from the pump to the hydraulic cylinder is neglected, the pump pressure p_p is equal to the cylinder pressure p_h . Applying the balance of mass then yields [1]

$$\frac{d}{dt}p_h = \frac{1}{\frac{V_p \rho_h}{\beta_p} + \frac{2\rho_h(V_{ci0} - A_{ci}x_s)}{\beta_{ci}}} (\dot{m}_p + 2A_{ci}v_s\rho_h). \quad (4)$$

Here, V_p is the volume of the piping, V_{ci0} is the cylinder volume for $x_s = 0$, and ρ_h is the density of oil (as a function of p_h). Moreover, β_p and β_{ci} are the effective bulk moduli of the oil in the corresponding hydraulic cavities, which are not equal due to the presence of flexible hydraulic hoses in the supply line between the pump and the cylinder. The pump mass flow \dot{m}_p can be modeled as

$$\dot{m}_p = -\rho_h V_{th} n_p \eta_{vol}, \quad (5)$$

with the displacement volume V_{th} of the pump, the volumetric efficiency $\eta_{vol}(p_h)$, and the pump speed n_p . Applying the balance of moment of momentum, the pump speed is given by

$$\frac{d}{dt}n_p = \frac{1}{2\pi J_p} (-\tau_{p,hm} - \tau_{fr} + \tau_{el}), \quad (6)$$

with the hydro-mechanic pump torque $\tau_{p,hm} = -\frac{V_{th}}{2\pi} \frac{(p_h - p_0)}{\eta_{hm}}$, where $\eta_{hm}(p_h)$ is the hydro-mechanic efficiency. Moreover, τ_{fr} is the friction torque and the electric torque τ_{el} of the motor is the control input to the system.

Remark 1. The servo-pump of the injection unit is speed-controlled by an inner controller implemented on the inverter, which utilizes τ_{el} as control input. Thus, the desired pump speed n_p^d serves as control input for the outer controller and (6) is used to estimate the required torque τ_{el} . The dynamics of the inverter and its inner control loop can be assumed to be ideal except for a significant time delay, which has to be addressed in the controller design.

The resulting fifth order model (1) - (6) is able to accurately describe the system behavior in a large operating range. For a model-based control strategy, it makes sense to analyze this model with respect to possible simplifications, which might reduce the overall model complexity. First, the friction force F_{fr} in (1) is neglected. This is reasonable because F_{fr} is small compared to the hydraulic forces acting on the pistons during the filling and packing phase, cf. [1].

It is well documented in literature that mechanical systems driven by a hydraulic cylinder often contain subsystems with significantly different dynamics, see, e.g., [38]. The fast subsystem is linked to the coupling between the hydraulic force $F_s = A_{ac}(p_{ac} - p_0) - 2A_{ci}(p_h - p_0)$ and the velocity v_s of the piston. From a control perspective, it is meaningful to eliminate this fast dynamics from the controller design model. To do so, the state transformation

$$[x_s, v_s, p_{ac}, p_h, n_p]^T \rightarrow [x_s, v_s, F_s, p_h, n_p]^T, \quad (7)$$

with F_s as described before, is applied to the mathematical model (1) - (6). This gives the dynamics of the fast subsystem in the form

$$\frac{d}{dt}v_s = \frac{1}{m_s}F_s \quad (8a)$$

$$\frac{d}{dt}F_s = \frac{\beta_{ac}}{x_0 + x_s + r_s(p_{ac} + \beta_{ac})}(-A_{ac}v_s - q_{no}) - \frac{2A_{ci}}{\frac{V_p\rho_h}{\beta_p} + \frac{2\rho_h(V_{ci0} - A_{ci}x_s)}{\beta_{ci}}}(\dot{m}_p + 2A_{ci}v_s\rho_h) \quad (8b)$$

while the slow dynamics is still given by (1a), (4), (6). This can be also checked by the eigenvalues of the linearized system for typical operating points. As expected, there is a conjugate complex eigenvalue, which is significantly faster than the other eigenvalues, and which can be attributed to v_s and F_s . Applying the singular perturbation theory yields the quasi-stationary solution of the fast subsystem (8) in the form

$$v_s = \left[\frac{A_{ac}\beta_{ac}}{x_0 + x_s + r_s(p_{ac} + \beta_{ac})} + \frac{4A_{ci}^2\rho_h}{\frac{V_p\rho_h}{\beta_p} + \frac{2\rho_h(V_{ci0} - A_{ci}x_s)}{\beta_{ci}}} \right]^{-1} \left(-\frac{\beta_{ac}}{x_0 + x_s + r_s(p_{ac} + \beta_{ac})}q_{no} - \frac{2A_{ci}}{\frac{V_p\rho_h}{\beta_p} + \frac{2\rho_h(V_{ci0} - A_{ci}x_s)}{\beta_{ci}}}\dot{m}_p \right), \quad (9)$$

$$p_{ac} = \frac{1}{A_{ac}}(2A_{ci}(p_h - p_0)) + p_0. \quad (10)$$

The final reduced model for the controller design then reads as

$$\frac{d}{dt}x_s = v_s \quad (11a)$$

$$\frac{d}{dt}p_h = \frac{1}{\frac{V_p\rho_h}{\beta_p} + \frac{2\rho_h(V_{ci0} - A_{ci}x_s)}{\beta_{ci}}}(\dot{m}_p(n_p) + 2A_{ci}v_s\rho_{ci}) \quad (11b)$$

$$\frac{d}{dt}n_p = \frac{1}{2\pi J_p}(-\tau_{p,hm} - \tau_{fr} + \tau_{el}), \quad (11c)$$

where v_s from (9) with (3), $\dot{m}_p(n_p)$ from (5), and p_{ac} from (10) are to be utilized.

To check the validity of this reduction step, the eigenvalues of the linearized reduced system are compared with the eigenvalues of the linearized complete system. E.g., during the filling phase with a typical

mold, the eigenvalues of the reduced model calculate as $\{-25.7, -7.47, -0.04\}$ and those of the complete model read as $\{-35.5 \pm 696I, -25.0, -7.49, -0.04\}$. Similar results are obtained for all other operating points.

A thorough proof of the validity of this reduction step would include checking the stability of the resulting boundary layer system, see, e.g., [39]. For the linearized system, this definitely holds true, which also applies locally to the nonlinear case. A systematic stability proof of the nonlinear boundary layer model is beyond the scope of this paper, which is why the feasibility of the reduced model is assessed by comparing the reduced with the complete model in simulations. Fig. 2 and Fig. 3 show the results of a typical injection experiment and a typical melt cushion experiment, respectively. Here, an identified mold conductance $c_{no}(x_s)$ is used for the injection experiment and $q_{no} = 0$ holds during the melt cushion experiment, see Sec. IV-B2. Furthermore, the measured torque τ_{el} serves as model input. It is clearly visible that the

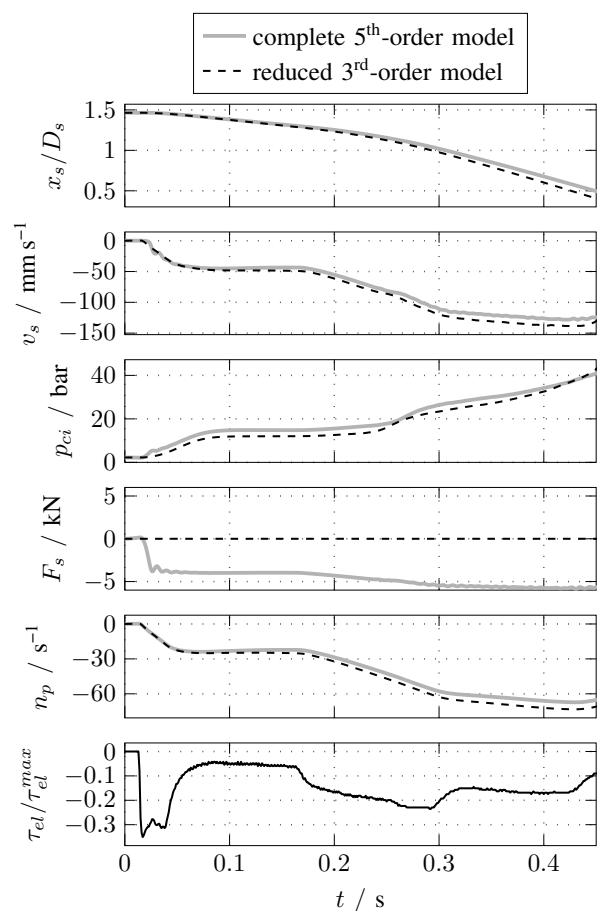


Fig. 2. Comparison of the reduced with the complete model: Simulation results of an injection experiment.

reduced model accurately captures the dynamic behavior of the complete model in these scenarios. The non-zero force F_s of the complete model mainly results from the friction force, which is neglected in the reduced model. This results in small stationary offsets of the remaining system states. This,

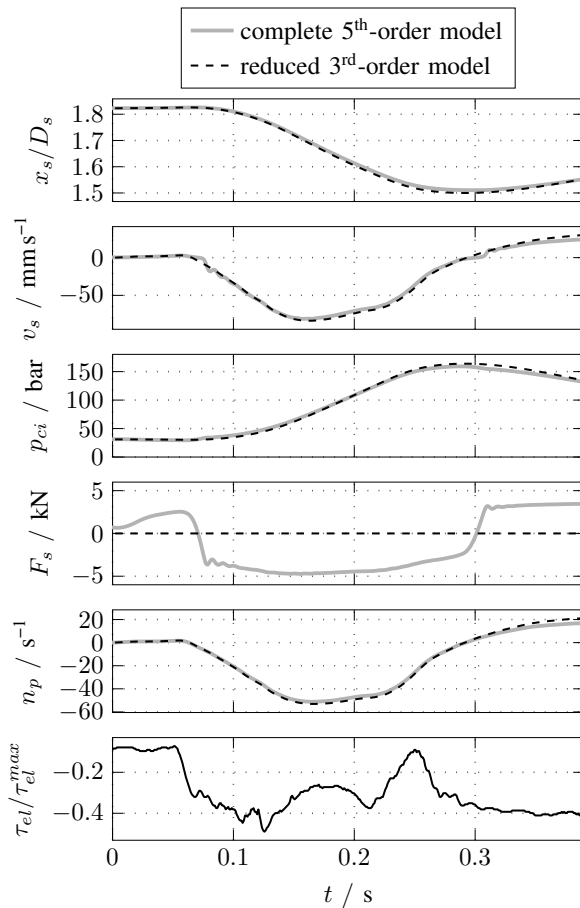


Fig. 3. Comparison of the reduced with the complete model: Simulation results of a melt cushion experiment with $q_{no} = 0$.

however, is no major drawback since stationary accuracy will be ensured by considering a possible model-plant mismatch in the controller design. Thus, the reduced model serves as a good basis for the subsequent controller design.

The reduced model (11) is abbreviated as

$$\dot{\mathbf{x}} = \mathbf{f}(\mathbf{x}, \tau_{el}, c_{no}), \quad (12)$$

with the state $\mathbf{x} = [x_s, p_h, n_p]^T$, the system input τ_{el} and the unknown input c_{no} .

Remark 2. The mathematical model (12) of the IMM is parametrized as follows: The areas, volumes and stiffness parameters of the IMM are taken from construction data. The parameters of the hydraulic fluid, the hydraulic hoses, and the parameters of the servo-pump are made available in the respective data sheets. The parameters β_0, β_1 , and β_2 of the polymer's bulk modulus are calculated from a complex Tait model. The parameters of the Tait model and the flow behavior index n of the utilized polymer can be found in the literature. The mass m_s and the friction force F_{fr} can be identified by measurements as described in [1]. These parameters, however, are not used in the reduced model and thus have no influence on the controller design. A discussion on the sensitivity of

the proposed control strategy to uncertainties in the model parameters is given in Sec. IV-C.

III. CONTROL STRATEGY

A. Control Task

In the present work, a common control strategy for the filling and packing phase of an injection process is developed. The different control tasks in these two phases are defined as follows: (i) During filling of the mold the velocity v_s of the screw should track a desired trajectory v_s^d . Experienced users typically try to set this trajectory in order to maintain a constant velocity of the melt front in the mold. This trajectory would ideally be parameterized as a function of the mold filling level instead of the time t . Because the mold filling level cannot be measured, it is typically parameterized as a function of the screw position x_s , i. e., $v_s^d = v_s^d(x_s)$. This parameterization guarantees that the same filling level (screw position) is reached, even if the velocity cannot be perfectly tracked due to system constraints or non-ideal controllers. During the filling phase it has to be ensured that the injection pressure p_h does not exceed a maximum pressure p_h^{max} to protect the mold and the injection unit. (ii) To completely fill the mold after the filling phase and to compensate for the shrinking of the cooling polymer in the mold, a desired pressure trajectory p_h^d has to be maintained in the packing phase. In contrast to the filling phase, this trajectory is parameterized as a function of time, i. e., $p_h^d = p_h^d(t)$. To keep the mechanical stress of the polymer below a critical limit, the screw velocity v_s is constrained by a velocity trajectory¹ $v_s \geq v_s^d(x_s)$ in this phase as well.

The limits of the actuator have to be taken into account during both phases. The physical constraint of the servo-drive in combination with the power electronics can be formulated as $|n_p| \leq n_p^{max}$ and $|\tau_{el}| \leq \tau_{el}^{max}$. Additionally, the slew rate of the rotational speed n_p has to be within a safety margin $\dot{n}_p^{min} \leq \frac{d}{dt}n_p \leq \dot{n}_p^{max}$ to avoid cavitation in the hydraulic system, in particular at the pump.

The control of the system is further complicated by the fact that the behavior of the mold, i. e., the volume flow q_{no} , is in general unknown. Another challenge in the control of the considered system is due to the significant time delay (mainly due to communication and processing time delay between the ECU and the inverter of the servo-pump), which can cause a significant deterioration of the closed-loop performance.

To solve this control task, a model-predictive control (MPC) strategy in combination with an estimation strategy for q_{no} is proposed in this paper.

B. Estimation of q_{no}

As discussed before, the control strategy should be applicable to any (unknown) mold and therefore, no model for the flow conductance c_{no} is available. Subsequently, an online estimator for the volume flow q_{no} is developed first, since it turned out that estimating q_{no} and calculating c_{no} with (3) results in a more robust estimation of the process

¹Please note that the velocity v_s has negative values during injection.

behavior. In addition to q_{no} also the measured pressure p_h is estimated because this gives additional degrees of freedom for the estimator design [38]. As there is no valuable a priori information available, the volume flow q_{no} is assumed to be constant but unknown, i. e., $\dot{q}_{no} = 0$. The estimator is basically a copy of the mathematical model (11b)

$$\frac{d}{dt}\hat{p}_h = \Phi_q(x_s, p_h)\hat{q}_{no} + \Phi_p(x_s, p_h)n_p - \chi_p \quad (13a)$$

$$\frac{d}{dt}\hat{q}_{no} = -\chi_q, \quad (13b)$$

adding the corrector terms χ_p and χ_q which serve as degrees of freedom for the estimator design. Here, the abbreviations Φ_q and Φ_p summarize the corresponding terms in (11). They are nonlinear functions of the measured quantities x_s and p_h . Introducing the estimation errors $\hat{e}_p = p_h - \hat{p}_h$ and $\hat{e}_q = q_{no} - \hat{q}_{no}$ yields the error system

$$\frac{d}{dt}\hat{e}_p = \Phi_q\hat{e}_q + \chi_p \quad (14a)$$

$$\frac{d}{dt}\hat{e}_q = \chi_q. \quad (14b)$$

For the design of the corrector terms, the stability of the error system (14) with $\hat{\mathbf{x}}_e = [\hat{e}_p, \hat{e}_q]^T$ is analyzed using the Lyapunov function candidate

$$W_e(\hat{\mathbf{x}}_e) = \frac{1}{2}\hat{e}_p^2 + \frac{1}{2\lambda_q}\hat{e}_q^2, \quad (15)$$

with the estimator parameter $\lambda_q > 0$. The change of W_e along a solution of (14) gives

$$\frac{d}{dt}W_e = \Phi_q\hat{e}_p\hat{e}_q + \chi_p\hat{e}_p + \frac{\chi_q}{\lambda_q}\hat{e}_q.$$

The choice

$$\chi_q = -\lambda_q\Phi_q\hat{e}_p \quad (16a)$$

$$\chi_p = -\lambda_p\hat{e}_p \quad (16b)$$

with $\lambda_p > 0$ renders $\dot{W}_e = -\lambda_p\hat{e}_p^2$ negative semi-definite. As $W_e(\hat{\mathbf{x}}_e) > 0$ is radially unbounded, the equilibrium $\hat{e}_p = \hat{e}_q = 0$ of (14) can be proven to be globally asymptotically stable by applying LaSalle's invariance principle [40].

The estimator (13) with (16) will be combined with an MPC strategy. It is clear that the choice of the estimator parameters λ_p and λ_q will influence the performance and stability of the overall closed-loop system. Simulation studies have shown that it is necessary to adapt the estimator dynamics in order to achieve the same high performance of the overall closed-loop system in the whole operating range. In particular, the estimator dynamics has to be reduced in operating points with low injection speed, i. e., for instance in the packing phase. Therefore, the corrector term χ_q from (16a) is changed to

$$\chi_q = -f(v_s)\lambda_q\Phi_q\hat{e}_p, \quad (17)$$

by means of

$$f(v_s) = \min\left\{1, \left(\frac{v_s}{v_{s,q1}}\right)^2 + f_{min}\right\}, \quad (18)$$

with the parameters $f_{min} > 0$ and $v_{s,q1} > 0$. A proof of the stability of the adapted estimator (13) with time-varying gain

(17) is given in App. A. The estimator (13) with (16b), (17) is implemented in discrete time by means of a 3rd-order Runge-Kutta integration method with the sampling time $T_s = 1$ ms.

In the subsequent model-predictive control strategy, it makes sense to utilize the estimated value \hat{c}_{no} of the conductivity c_{no} of the mold model instead of \hat{q}_{no} , since this allows to take into account the influence of the (predicted) pressure p_{ac} on the predicted volume flow into the mold. The estimated value \hat{c}_{no} is directly calculated by utilizing (3) in the form

$$\hat{c}_{no} = \frac{\hat{q}_{no}}{(p_{ac} - p_0)^{\frac{1}{n}}}, \quad (19)$$

with p_{ac} from (10) using the measured pressure p_h .

C. Formulating the Optimal Control Problem

In this section, the control task defined in Sec. III-A is formulated as an optimal control problem (OCP), which will be solved on a receding horizon. Before this can be done, some preliminary discussion is required.

The control task in the filling phase is defined as a velocity tracking control problem, where the desired trajectory v_s^d is defined as a function of the screw position x_s . Direct measurement of the velocity v_s is not available in the real system. Thus, it makes sense to reformulate the velocity control task in the form of a position control task, with the desired position x_s^d calculated by the solution of

$$\frac{d}{dt}x_s^d = v_s^d(x_s^d), \quad x_s^d(0) = x_{s,0}, \quad (20)$$

where $x_{s,0}$ is the screw position at the beginning of the injection cycle. This ODE is numerically solved yielding the desired trajectory $x_s^d(t)$.

As mentioned before, the actuator (servo-pump and inverter) has a non-negligible time delay (≈ 2 ms) due to the bus communication and internal data processing. Furthermore, the delay due to the solution of the optimization problem is basically equal to the sampling time $T_s = 1$ ms. Thus, a total time delay of $T_{td} = N_{td}T_s = 3T_s = 3$ ms passes before a measured control error is reflected in a reaction of the system. Without considering this time delay, the closed-loop system can become unstable, in particular during the pressure-controlled phase. To approximately take into account this time delay the subsystem

$$\dot{\mathbf{z}} = \mathbf{f}_z(\mathbf{z}, n_p, c_{no}), \quad (21)$$

which is derived from (11a) and (11b) with $\mathbf{z} = [x_s, p_h]^T$, is extrapolated over the time delay. For this, (21) is integrated via the explicit Euler method with the sampling time T_s starting from the currently measured position x_s and hydraulic pressure p_h as initial values, the previously calculated control inputs $n_{p,k-3}^d, n_{p,k-2}^d, n_{p,k-1}^d$, which already had been sent to the inverter, and the current estimate $\hat{c}_{no,k}$. Since it can be assumed that the speed controller of the pump works well, no prediction of the speed dynamics (11c) is required and the predicted speed $\hat{n}_{p,k+N_{td}}$ can be set to the value calculated by the MPC, i. e., $n_{p,k-1}^d$. This yields a prediction

$$\hat{\mathbf{x}}_{k+N_{td}} = [\hat{x}_{s,k+N_{td}}, \hat{p}_{h,k+N_{td}}, \hat{n}_{p,k+N_{td}}]^T,$$

which will be used as the initial value for the OCP of the MPC. For a more detailed discussion of this time delay compensation method, see, e. g., [41].

The model (12) is utilized for the prediction step in the MPC strategy. A discrete-time approximation with sampling time T_p of (12) is utilized by applying the explicit Euler method, yielding

$$\mathbf{x}_{j+1|k} = \mathbf{x}_{j|k} + T_p \mathbf{f}(\mathbf{x}_{j|k}, \tau_{el,j|k}, \hat{c}_{no,k}). \quad (22)$$

Therein, $\mathbf{x}_{j|k}$ describes the predicted value of \mathbf{x} at time $t = (k + N_{td})T_s + jT_p$ based on measurements up to kT_s and $\mathbf{x}_{0|k}$ is initialized with $\hat{\mathbf{x}}_{k+N_{td}}$ as described before. Fig. 4 shows the discretization steps for the extrapolation phase as well as for the prediction step.

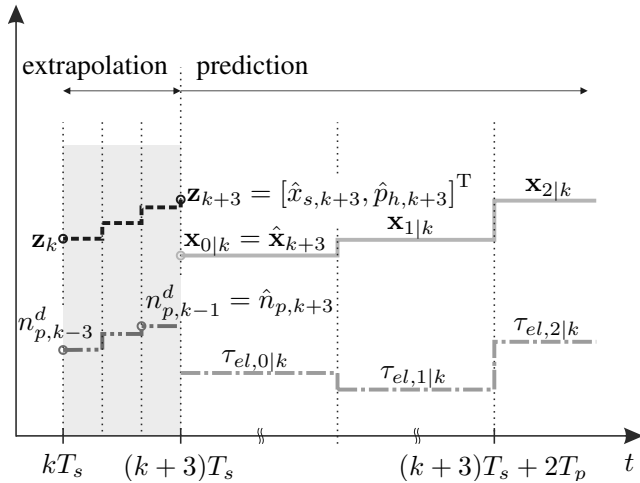


Fig. 4. Timing of the MPC.

It is well documented in literature that the control performance and stability of an MPC is strongly related to sufficiently long prediction horizons NT_p , see, e. g., [42]. The number of prediction steps N is, however, limited by the computational effort. If the sampling time T_p of the prediction model is chosen to be a multiple of T_s , e. g., $T_p = N_p T_s$, longer prediction horizons can be achieved while keeping the computational effort limited. The suitable choice of N_p is related to the stability and accuracy of the prediction model (22) and will be discussed later.

Due to the unknown load, i. e., the behavior of the mold, it is possible that the constraints discussed in Sec. III-A (e. g., pressure and speed limits) cannot be exactly satisfied at every time step. To avoid an infeasible OCP in these cases, the inequality constraints are taken into account in the form of soft constraints utilizing a penalty function. E. g., the penalty function $P_{n_p}(n_{p,j|k})$ for the pump speed n_p is formulated as

$$P_{n_p}(n_{p,j|k}) = \frac{\Gamma_{n_p}}{2} \begin{cases} (n_{p,j|k} - n_p^{min})^2 & n_{p,j|k} < n_p^{min} \\ (n_{p,j|k} - n_p^{max})^2 & n_{p,j|k} > n_p^{max} \\ 0 & \text{else,} \end{cases} \quad (23)$$

with the maximum and minimum values n_p^{max} and n_p^{min} , respectively, and the weight $\Gamma_{n_p} > 0$. The penalty functions

$P_{\tau_{el}}$, P_{p_h} , P_{n_p} , and $P_{v_s,j}$ for the quantities τ_{el} , p_h , \dot{n}_p , and v_s are defined in a similar way.

With these preliminaries, the OCP reads as

$$\min_{\substack{\mathbf{x}_{0|k}, \dots, \mathbf{x}_{N|k}, \\ \tau_{el,0|k}, \dots, \tau_{el,N|k}}} \sum_{j=0}^N J_j \quad (24a)$$

$$\text{s.t.} \quad \mathbf{x}_{j+1|k} = \mathbf{x}_{j|k} + T_p \mathbf{f}(\mathbf{x}_{j|k}, \tau_{el,j|k}, \hat{c}_{no,k}), \quad (24b)$$

$$j = 0, \dots, N - 1 \quad (24c)$$

$$\mathbf{x}_{0|k} = \hat{\mathbf{x}}_{k+N_{td}} \quad (24c)$$

Therein, the cost function J_j is differently defined for the filling and packing phase due to the different control tasks. In the filling phase, the cost function takes the form

$$J_j^{fill} = \frac{1}{2} Q_{x_s} (\bar{x}_{s,j|k}^d - x_{s,j|k})^2 \quad (25)$$

$$+ \frac{1}{2} R_{\tau_{el}} (\tau_{el,j|k} - \tau_{el,j-1|k})^2 + P_{\tau_{el}}(\tau_{el,j|k})$$

$$+ P_{p_h}(p_{h,j|k}) + P_{n_p}(n_{p,j|k})$$

$$+ P_{\dot{n}_p}((n_{p,j|k} - n_{p,j-1|k})/T_p)$$

$$+ P_{v_s,j}((x_{s,j|k} - x_{s,j-1|k})/T_p),$$

with the positive weighting factors $Q_{x_s} > 0$, $R_{\tau_{el}} > 0$. While the first term obviously penalizes the deviations of the screw position from its desired position $\bar{x}_{s,j|k}^d$, the second term is introduced to improve the smoothness of τ_{el} .

Remark 3. J_0^{fill} differs slightly since the trajectory error as well as the penalty functions for the initial point $\mathbf{x}_{0|k}$ can be omitted. Thus, $J_0^{fill} = \frac{1}{2} R_{\tau_{el}} (\tau_{el,0|k} - \tau_{el,-1|k})^2 + P_{\tau_{el}}(\tau_{el,0|k})$ remains. Here, $\tau_{el,-1|k}$ is introduced to ensure the smoothness of the control input $\tau_{el,0|k}$ in reference to the last MPC step at $k - 1$.

In (25) an adjusted desired position $\bar{x}_{s,j|k}^d$ is introduced in order to prevent very large tracking errors, e. g., when the pressure limit is hit. To do so, $\bar{x}_{s,j|k}^d$ is defined as

$$\bar{x}_{s,j|k}^d = \max(x_s^d((k + N_{td})T_s + jT_p), x_{s,k} - e_s^{max}),$$

which limits the tracking error in (25) to e_s^{max} referred to the currently measured position x_s .

The penalty function P_{v_s} requires a little more explanation. As discussed before, the operator input is a desired velocity as a function of x_s , i. e., $v_s^d(x_s)$. The screw velocity is closely related to the volume flow into the mold, and the operator chooses $v_s^d(x_s)$ in a way that the resulting product meets its specification. It is well documented that if the mold is filled with higher speed the product quality can significantly reduce. In a system without constraints, tracking the desired trajectory x_s^d would of course keep the desired speed limit. If, however, the desired trajectory cannot be tracked, e. g., due to hitting the pressure limit, a pronounced tracking error can occur. If, after a certain time, e. g., due to a change of the mold behavior, these limits are no longer active, the controller tries to catch up with the desired position x_s^d . This may result in injection

speeds $|v_s|$ which are larger than the desired speed $|v_s^d(x_s)|$. Now, the penalty function P_{v_s} is defined as

$$P_{v_s,j}(v_{s,j|k}) = \begin{cases} \Gamma_{v_s,j}(v_{s,j|k} - v_s^d(x_{s,j|k}))^2 & v_{s,j|k} < v_s^d(x_{s,j|k}) \\ 0 & \text{else,} \end{cases} \quad (26)$$

with the abbreviation $v_{s,j|k} = (x_{s,j|k} - x_{s,j-1|k})/T_p$ and the time-varying weight $\Gamma_{v_s,j} > 0$. Thus, P_{v_s} in the form (26) penalizes injection speeds of the screw faster than the desired speed $|v_s^d|$.

The cost function for the packing phase can be formulated in a similar way by

$$J_j^{pack} = \frac{1}{2} Q_{p_h,j} (p_h^d((k + N_{td})T_s + jT_p) - p_{h,j|k})^2 + \frac{1}{2} R_{\tau_{el}} (\tau_{el,j|k} - \tau_{el,j-1|k})^2 + P_{\tau_{el}} (\tau_{el,j|k}) + P_{n_p} (n_{p,j|k}) + P_{\hat{n}_p} ((n_{p,j|k} - n_{p,j-1|k})/T_p) + P_{v_s} (v_{s,j|k}), \quad (27)$$

with the time-varying weight $Q_{p_h,j} > 0$. As a matter of fact, the penalty function P_{p_h} for the pressure is not relevant in this phase.

D. Implementation of the MPC with Riccati Recursion

To efficiently solve the OCP (24) the iterative algorithm introduced by Diehl [43] is employed and extended. This algorithm calculates a suboptimal solution on a finite receding prediction horizon. For this, the cost function is reformulated by introducing the time-shifted variables of $\mathbf{x}_{j|k}$ and $\tau_{el,j|k}$ in the form

$$\mathbf{y}_{j+1|k} = \mathbf{x}_{j|k} \quad (28a)$$

$$z_{j+1|k} = \tau_{el,j|k}. \quad (28b)$$

Thus, the cost function J_j of (25) or (27), respectively, only depends on $\tau_{el,j|k}$ and the augmented state

$$\mathbf{s}_{j|k} = [\mathbf{x}_{j|k}, \mathbf{y}_{j|k}, z_{j|k}]^T \quad (29)$$

at the time index j .

Remark 4. Subsequently, the notation

$$\frac{\partial \zeta}{\partial \xi}(\xi_{j|k}) = \left. \frac{\partial \zeta(\xi)}{\partial \xi} \right|_{\xi=\xi_{j|k}}$$

for the Jacobian of $\zeta(\xi)$ with respect to ξ evaluated at $\xi = \xi_{j|k}$ will be used. Note that ζ and ξ can also be a scalar function or variable, respectively.

For the iterative solution of the OCP, the nonlinear constraint (24b) is linearized in the iteration l around the optimal trajectory $(\mathbf{s}_{j|k}^{l-1}, \tau_{el,j|k}^{l-1})$ obtained in the previous iteration $l-1$, i. e.,

$$\begin{aligned} \mathbf{x}_{j+1|k} &= \mathbf{x}_{j+1|k}^{l-1} + \Delta \mathbf{x}_{j+1|k}^l \\ &\approx \mathbf{x}_{j|k}^{l-1} + T_p \mathbf{f}(\mathbf{x}_{j|k}^{l-1}, \tau_{el,j|k}^{l-1}, \hat{c}_{no,k}) \\ &\quad + \Phi_{x,j|k}^l \Delta \mathbf{x}_{j|k}^l + \Gamma_{x,j|k}^l \Delta \tau_{el,j|k}^l, \end{aligned} \quad (30)$$

with $\Delta \mathbf{x}_{j|k}^l = \mathbf{x}_{j|k}^l - \mathbf{x}_{j|k}^{l-1}$ and $\Delta \tau_{el,j|k}^l = \tau_{el,j|k}^l - \tau_{el,j|k}^{l-1}$. Here, the abbreviations

$$\Phi_{x,j|k}^l = \mathbf{I} + T_p \frac{\partial \mathbf{f}}{\partial \mathbf{x}}(\mathbf{x}_{j|k}^{l-1}, \tau_{el,j|k}^{l-1}, \hat{c}_{no,k})$$

$$\Gamma_{x,j|k}^l = T_p \frac{\partial \mathbf{f}}{\partial \tau_{el}}(\mathbf{x}_{j|k}^{l-1}, \tau_{el,j|k}^{l-1}, \hat{c}_{no,k}),$$

with the identity matrix \mathbf{I} , are utilized, which have to be calculated for each prediction step $j = 0, \dots, N-1$ and in each iteration $l = 1, \dots, N_{it}$. To reduce the computational effort for a real-time capable implementation, the derivatives in $\Phi_{x,j|k}^l, \Gamma_{x,j|k}^l$ are calculated for the first iteration $l = 1$ and for the starting point $\mathbf{x}_{0|k}, \tau_{el,0|k}$ only and are kept constant, i. e., $\Phi_{x,j|k}^l = \Phi_{x,0|k}^1 = \Phi_{x,k}^1, \Gamma_{x,j|k}^l = \Gamma_{x,0|k}^1 = \Gamma_{x,k}^1$. It has been verified by simulation studies that this simplification yields sufficiently accurate results of the prediction model within the prediction horizon NT_p . The resulting equality constraint (30) can then be abbreviated as

$$\mathbf{c}_{x,j+1|k}^{l-1} + \Delta \mathbf{x}_{j+1|k}^l - \Phi_{x,k}^1 \Delta \mathbf{x}_{j|k}^l - \Gamma_{x,k}^1 \Delta \tau_{el,j|k}^l = \mathbf{0}, \quad (31)$$

with $\mathbf{c}_{x,j+1|k}^{l-1} = \mathbf{x}_{j+1|k}^{l-1} - \mathbf{x}_{j|k}^{l-1} - T_p \mathbf{f}(\mathbf{x}_{j|k}^{l-1}, \tau_{el,j|k}^{l-1}, \hat{c}_{no,k})$. The (already linear) dynamics of the augmented state (28) can be formulated similarly as

$$\mathbf{c}_{y,j+1|k}^{l-1} + \Delta \mathbf{y}_{j+1|k}^l - \Delta \mathbf{x}_{j|k}^l = \mathbf{0} \quad (32a)$$

$$\mathbf{c}_{z,j+1|k}^{l-1} + \Delta z_{j+1|k}^l - \Delta \tau_{el,j|k}^l = 0, \quad (32b)$$

with $\mathbf{c}_{y,j+1|k}^{l-1} = \mathbf{y}_{j+1|k}^{l-1} - \mathbf{x}_{j|k}^{l-1}$ and $\mathbf{c}_{z,j+1|k}^{l-1} = z_{j+1|k}^{l-1} - \tau_{el,j|k}^{l-1}$. Putting the results of (31) and (32) together, the following equivalent formulation of the constraints (28), (30) is given by

$$\mathbf{c}_{j+1|k}^{l-1} + \Delta \mathbf{s}_{j+1|k}^l - \Phi_k^1 \Delta \mathbf{s}_{j|k}^l - \Gamma_k^1 \Delta \tau_{el,j|k}^l = \mathbf{0}. \quad (33)$$

The cost function J_j is approximated in every iteration l by a Taylor series of second order in the form

$$\begin{aligned} J_j^l &= J_j(\mathbf{s}_{j|k}^{l-1}, \tau_{el,j|k}^{l-1}) + (\mathbf{g}_{j|k}^l)^T \Delta \mathbf{s}_{j|k}^l \\ &\quad + d_{j|k}^l \Delta \tau_{el,j|k}^l + \Delta \tau_{el,j|k}^l (\mathbf{b}_{j|k}^l)^T \Delta \mathbf{s}_{j|k}^l \\ &\quad + \frac{1}{2} (\Delta \mathbf{s}_{j|k}^l)^T \Omega_{j|k}^l \Delta \mathbf{s}_{j|k}^l + \frac{1}{2} R_{j|k}^l (\Delta \tau_{el,j|k}^l)^2 \end{aligned} \quad (34)$$

with

$$(\mathbf{g}_{j|k}^l)^T := \frac{\partial J_j}{\partial \mathbf{s}_{j|k}}(\mathbf{s}_{j|k}^{l-1}, \tau_{el,j|k}^{l-1}) \quad (35)$$

$$d_{j|k}^l := \frac{\partial J_j}{\partial \tau_{el,j|k}}(\mathbf{s}_{j|k}^{l-1}, \tau_{el,j|k}^{l-1})$$

$$(\mathbf{b}_{j|k}^l)^T := \frac{\partial^2 J_j}{\partial \mathbf{s}_{j|k} \partial \tau_{el,j|k}}(\mathbf{s}_{j|k}^{l-1}, \tau_{el,j|k}^{l-1})$$

$$\Omega_{j|k}^l := \frac{\partial^2 J_j}{\partial \mathbf{s}_{j|k}^2}(\mathbf{s}_{j|k}^{l-1}, \tau_{el,j|k}^{l-1})$$

$$R_{j|k}^l := \frac{\partial^2 J_j}{\partial \tau_{el,j|k}^2}(\mathbf{s}_{j|k}^{l-1}, \tau_{el,j|k}^{l-1}).$$

Remark 5. The initial point $\mathbf{x}_{0|k}$, included in $\mathbf{s}_{0|k}^l$, is determined by the measured and predicted initial state $\hat{\mathbf{x}}_{k+N_{td}}$. This is why any weighting of this state itself can be omitted

and $\mathbf{g}_{0|k}^l, \mathbf{\Omega}_{0|k}^l$ are set to zero in J_0^l as discussed before. As a consequence, $\mathbf{y}_{0|k}$ included in $\mathbf{s}_{0|k}^l$ is not used and can be set to zero, too. The initial value $z_{0|k}$ has to be recalled from a previous solution of the MPC to still ensure smoothness of the (virtual) control input $\tau_{el,0|k}^l$ relative to the last MPC-step $\tau_{el,0|k-1}^*$, i. e., $z_{0|k} = \tau_{el,0|k-N_p}^*$ to match the time grid $T_p = N_p T_s$. Furthermore, the input $\Delta \tau_{el,N|k}^l$ does not have an influence on the states within the optimization horizon NT_p . To eliminate this variable from the OCP, $\mathbf{b}_{N|k}^l, \mathbf{d}_{N|k}^l, \mathbf{R}_{N|k}^l$ are set to zero in J_N^l .

Thus, the resulting optimization problem can be formulated as

$$\begin{aligned} \min_{\Delta \mathbf{s}_{0|k}^l, \dots, \Delta \mathbf{s}_{N|k}^l} \sum_{j=0}^N J_j^l \quad (36a) \\ \text{s.t. } \mathbf{c}_{j+1|k}^{l-1} + \Delta \mathbf{s}_{j+1|k}^l - \mathbf{\Phi}_k \Delta \mathbf{s}_{j|k}^l - \mathbf{\Gamma}_k \Delta \tau_{el,j|k}^l = \mathbf{0}, \quad (36b) \\ j = 0, \dots, N-1 \\ \Delta \mathbf{s}_{0|k}^l = \mathbf{0}. \quad (36c) \end{aligned}$$

Summarizing, the original OCP (24) has been reformulated to the iterative solution of the quadratic program (QP) (36), where the coefficients of the cost function and the equality constraints depend on the states $\mathbf{s}_{j|k}^{l-1}$ and the control input $\tau_{el,j|k}^{l-1}$. This QP is solved by a Riccati recursion scheme, which is briefly summarized in App. B.

The results of this MPC are the optimal values $\mathbf{x}_{j|k}^*$ and $\tau_{el,j|k}^*$. As briefly discussed in Sec. II, a speed controller is already implemented on the inverter of the servo-pump. The dynamics of this speed control loop is rather fast and thus can be considered ideal for the control of the filling and packing phase. The required desired rotational speed $n_{p,k}^d$ for the inverter is thus interpolated at $t = T_s$ from the optimum value $n_{p,j|k}^*$ (part of $\mathbf{x}_{j|k}^*$) of the MPC strategy. Please note that the incorporation of the servo-drive dynamics (11c) into the MPC is only done to be able to take the limits of the torque τ_{el} into account.

IV. VALIDATION OF THE CONTROL STRATEGY

In this section the proposed control strategy is validated by simulation and measurements. First, the estimation of q_{no} is investigated. Due to the fact that the volume flow cannot be measured in the experiment, simulation results are shown to compare the estimated volume flow with the simulated one. The performance of the closed-loop system including the MPC is validated by presenting the results of measurement campaigns conducted on a real injection molding machine.

A. Validation of the estimator

For parameter tuning and validation of the proposed estimator (13) with (16b) and (17), the estimated quantities are compared with the corresponding quantities of the full simulation model presented in Sec. II and described in detail in [1]. Additionally, realistic measurement noise is added to the pressure p_h and the position x_s . The chosen parameters of

the estimator are given in Tab. III of App. C. By means of λ_p and λ_q the dynamics of the estimator can be adjusted. On the one hand the estimator should be fast enough to track rapid changes of q_{no} , on the other hand high dynamics amplifies the measurement noise and may deteriorate the performance of the overall closed-loop system including the MPC. For this reason, $v_{s,q1}$ and f_{min} are chosen to reduce the dynamics for operating points with low injection speeds.

Fig. 5 and Fig. 6 show the estimated pressure \hat{p}_h and volume flow \hat{q}_{no} for two experimental setups. Here, q_{ref} is the volume flow, which can be established at the maximum injection speed $|v_s|$ of the specific injection unit. The results

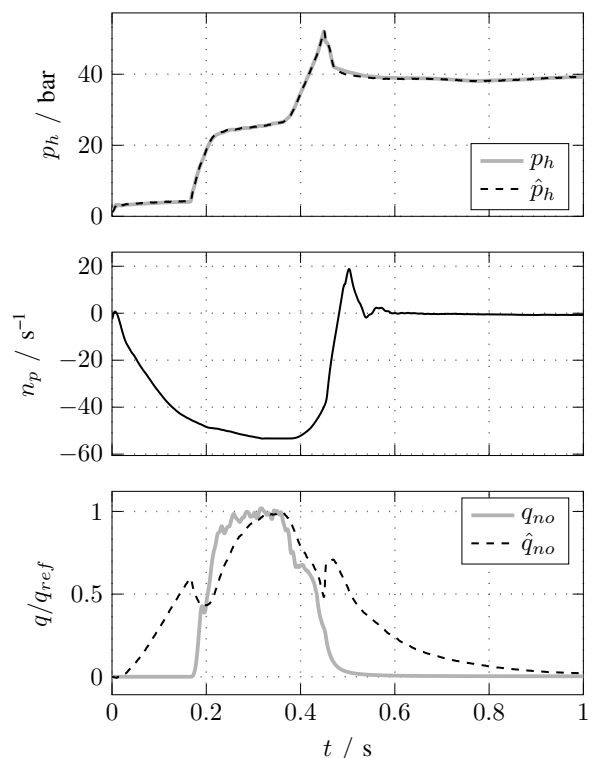


Fig. 5. Validation of the load estimator: Simulation results of a form injection scenario.

of a typical form injection experiment are depicted in Fig. 5. While the estimation error \hat{e}_p is almost zero, the estimation \hat{q}_{no} has remarkable deviations from the volume flow q_{no} into the mold. The reason for these deviations are as follows: (i) From $t = 0$ s to 0.2 s, the non-return valve is still open. In this case, liquid polymer can flow back at the screw and no pressure build-up takes place in the antechamber. This operation case is not covered by the model (11) utilized for the controller and estimator design. For this reason, the estimated volume flow \hat{q}_{no} is the sum of the volume flow into the mold and of this leakage flow. (ii) From $t = 0.2$ s to 0.45 s, the non-return valve is closed and the form is filled with \hat{q}_{no} close to q_{no} . (iii) During the packing phase, i. e., $t > 0.45$ s, the screw velocity v_s is almost zero and the estimator feedback gain is reduced for stability reasons of the overall closed-loop system. This results in an estimation error due to the slower estimator dynamics.

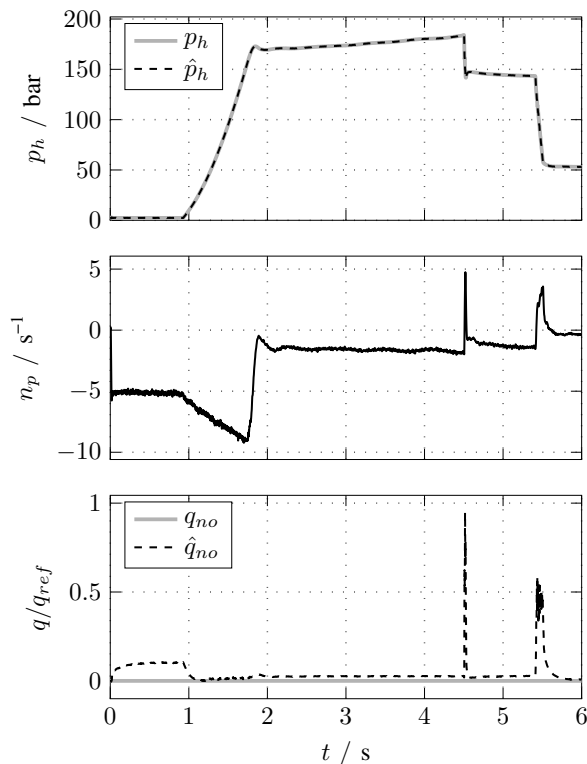


Fig. 6. Validation of the load estimator: Simulation results of a melt cushion scenario.

Fig. 6 shows the simulation results of a so-called melt cushion experiment, where the nozzle is closed manually and the polymer inside the enclosed antechamber is compressed. This experiment is a worst-case scenario for the controller and can occur, if, e.g., the runner freezes too early or it is clogged. The melt-cushion experiment can also be used to test the control performance in the pressure-controlled phase, see Sec. IV-B2. Clearly, $q_{no} = 0$ holds in this case. Again, the estimated value $\hat{q}_{no} \neq 0$ accounts for the open non-return valve at the beginning. The non-return valve closes at $t = 0.9$ s. The non-zero estimated volume flow \hat{q}_{no} then represents the leakages in the hydraulic system. For the rapid movements at $t = 4.5$ s and $t = 5.5$ s, the peaks in the estimated volume flow are due to the neglected inertia of the moving mass m_s .

These and further simulation results show that the proposed load estimator exhibits a good performance in all operating points and gives reasonable estimates \hat{q}_{no} for the volume flow q_{no} . It should be mentioned again that the main reason for utilizing an estimator for the unknown load volume flow is to achieve stationary accuracy of the closed-loop system in combination with the MPC. Thus, the focus of this estimator is not on estimating q_{no} as accurate as possible but to establish a stable closed-loop system with stationary accuracy.

B. Experimental Validation

The overall control strategy was experimentally validated by a number of different measurement campaigns. To do so,

a *dSPACE* real-time rapid-prototyping platform¹ was used to implement the MPC and the estimator at a sampling time of $T_s = 1$ ms. The connection to a state-of-the-art injection molding machine was carried out by an *EtherCAT* bus system. The performance of the proposed MPC is compared with the state-of-the-art controller (PID-based control strategy with trajectory planning that takes into account the limits of the injection molding machine, and a heuristic method to meet the pressure limits during the injection process). Polypropylene was used in the experiments with a temperature of 220 °C.

The parameters of the MPC were tuned by means of simulation studies in advance. Tab. IV in App. C shows the final parameter set. The sampling time of $T_s = 1$ ms has proven advantageous for the considered injection molding machine. The maximum sampling time of the discrete-time approximation $T_p = N_p T_s$ is limited by the stability of the chosen integration algorithm (22) for the model (11). The prediction horizon NT_p is chosen according to the actuator dynamics, i. e., at minimum the time which is required to reach maximum drive speed from standstill. As a consequence, the maximum number of iterations N_{it} used in the termination criterion of the MPC algorithm has to be selected according to the given computational power to restrict the computation time to T_s . The weights of the cost function are tuned in the following way: (i) The weights of the trajectory error Q_{x_s} and $Q_{p_{h,j}}$ are chosen together with $R_{\tau_{el}}$ in the unconstrained case. Here, a trade-off between the closed-loop dynamics and the smoothness of the control input has to be found. (ii) The weight of every single penalty function is tuned subsequently to appropriately meet the corresponding constraint.

1) *Form Injection*: The measurement results of a typical form injection experiment with the MPC is shown in Fig. 7. The desired screw velocity v_s^d at the beginning of the cycle is chosen at almost maximum speed to quickly reach the pressure limit. Then, the speed is reduced to validate the performance of the controller during the injection close to the pressure limit. After the mold is filled, the pressure-controlled phase with $p_h^d = 30$ bar starts at a position-dependent switch-over point. Thus, this point varies with the actual injection speed. The set-point n_p^d for the drive controller and the measured drive speed n_p are depicted in Fig. 7 as well. In addition to the minimum and maximum velocity also the constraints of the drive's acceleration are shown in two relevant situations, highlighted by the shaded areas. These limits are chosen asymmetrical to obtain a good compromise of system dynamics and protection of the pump when sucking oil from the tank or the cylinder. The primary control objective, i. e., tracking the desired velocity $v_s(x_s)$, is very well fulfilled. From $t = 0$ s to 0.06 s the injection molding machine is accelerating with the maximum allowed acceleration and hence, a tracking error is present. At $t = 0.18$ s, the flow resistance of the mold rises rapidly, causing a steep pressure rise and subsequent a drop in the velocity v_s . Due to the time delay this velocity drop is inevitable, but the desired velocity is reached again already a few milliseconds after the pressure rise. Additionally, the resulting torque τ_{el}^* of the MPC is compared with the measured

¹Freescale QorIQ P5020, dual-core, 2 GHz

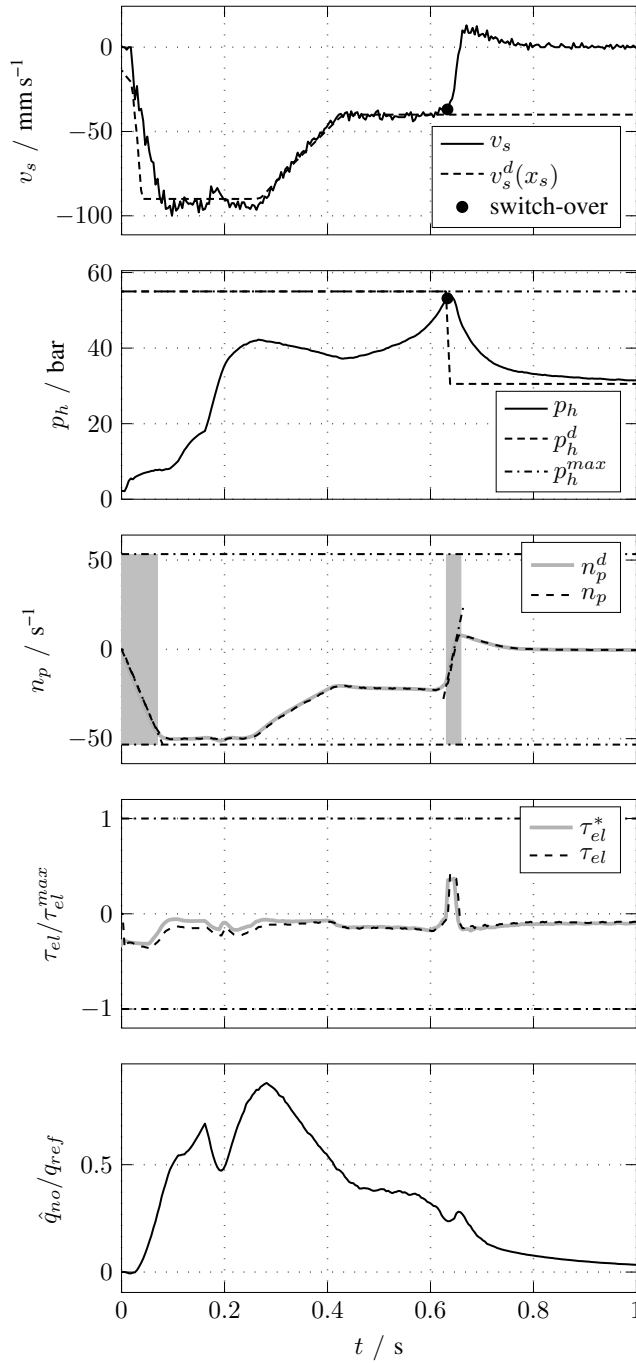


Fig. 7. Measurement results: Form injection experiment with MPC and $p_h^{max} = 55$ bar.

torque τ_{el} showing good accordance. In this specific test case, the torque limit is never reached. This is why the drive acceleration is the relevant limit to be considered. For the sake of completeness, the estimated volume flow \hat{q}_{no} is also shown for this experiment.

In Fig. 8, the closed-loop performance of the proposed MPC is compared with the industrial state-of-the-art (SOA) controller by means of the same experiment as shown in

Fig. 7. It is obvious that the MPC can better exploit the

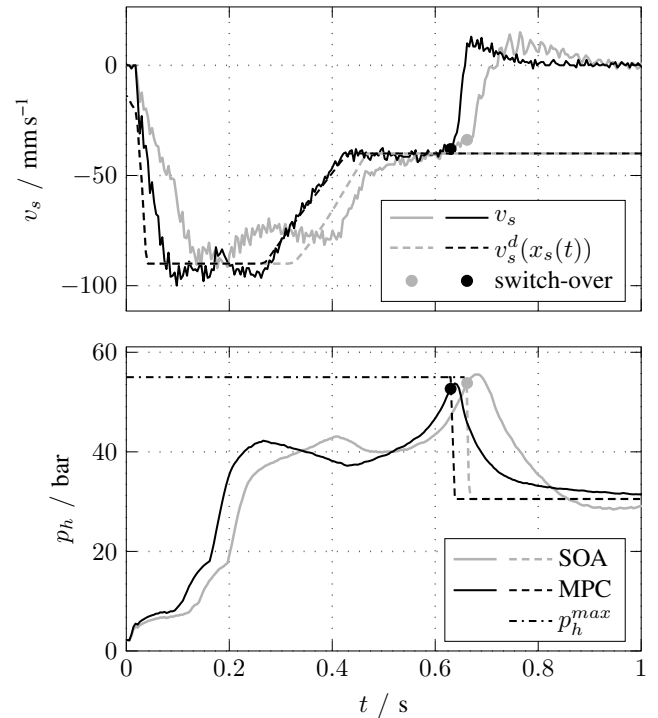


Fig. 8. Measurement results: Comparison of the state-of-the-art (SOA) controller with MPC for the form injection experiment with $p_h^{max} = 55$ bar.

full actuator dynamics and accelerates faster than the SOA controller. After the pressure rises steeply at $t \approx 0.2$ s, the velocity shows a significant tracking error for the SOA controller. Furthermore, after the switch-over to the pressure-controlled phase at $t > 0.65$ s the MPC reacts faster causing less overshoot and a faster decrease of the pressure.

To investigate the influence of the pressure limit during the injection the same experiment was conducted while gradually reducing the pressure limit. Fig. 9 and Fig. 10 show the results for three injection cycles with different pressure limits for both controllers. The drawbacks of the SOA controller compared to the proposed MPC can be summarized as follows:

- The injection speed $|v_s|$ drops considerably at $t = 0.2$ s due to the steep pressure rise although the pressure is well below the limit p_h^{max} .
- From $t = 0.4$ s to 0.6 s the velocity constraint is violated severely.
- During the experiment with pressure limit $p_h^{max} = 40$ bar, this limit is violated by almost 10 bar at $t = 0.7$ s to 0.8 s despite the lower injection speed $|v_s|$.

Fig. 10 demonstrates that with the proposed MPC concept the velocity constraint is almost never exceeded while the injection is as fast as possible. Additionally, the pressure limit is never exceeded by more than 5 bar.

To further study the control performance of the MPC, experiments with different molds, i.e., with a different behavior of the flow resistance, were conducted. In Fig. 11, the results of injection experiments with the same injection profile $v_s^d(x_s)$

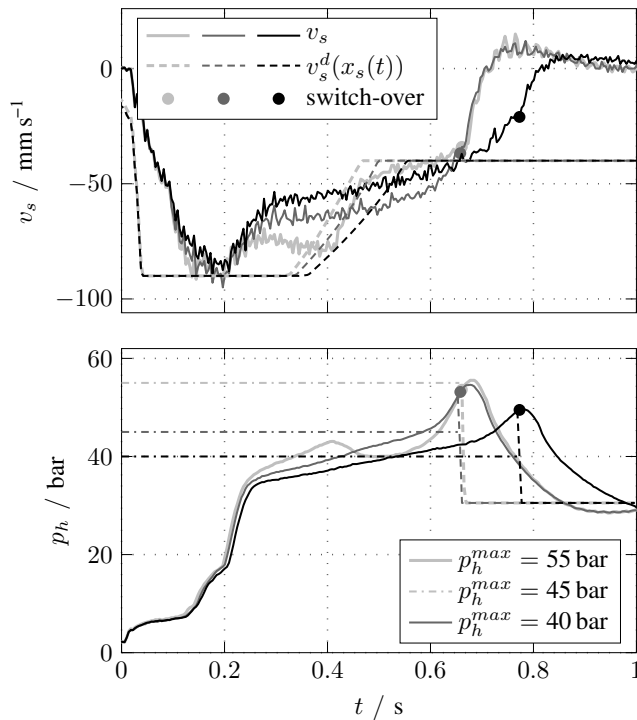


Fig. 9. Measurement results: Form injection experiments with different levels of the pressure limit with the state-of-the-art (SOA) controller.

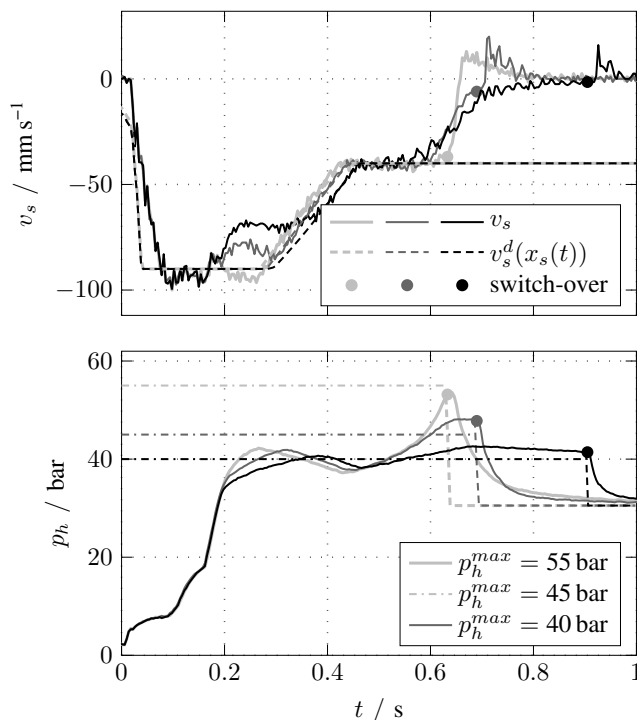


Fig. 10. Measurement results: Form injection experiments with different levels of the pressure limit with the MPC.

as in Fig. 7 but with three different molds are compared. In summary, it can be seen that the MPC shows a good control performance during the filling phase, independent of the used mold without the need for reconfiguring the controller or adapting the controller parameters.

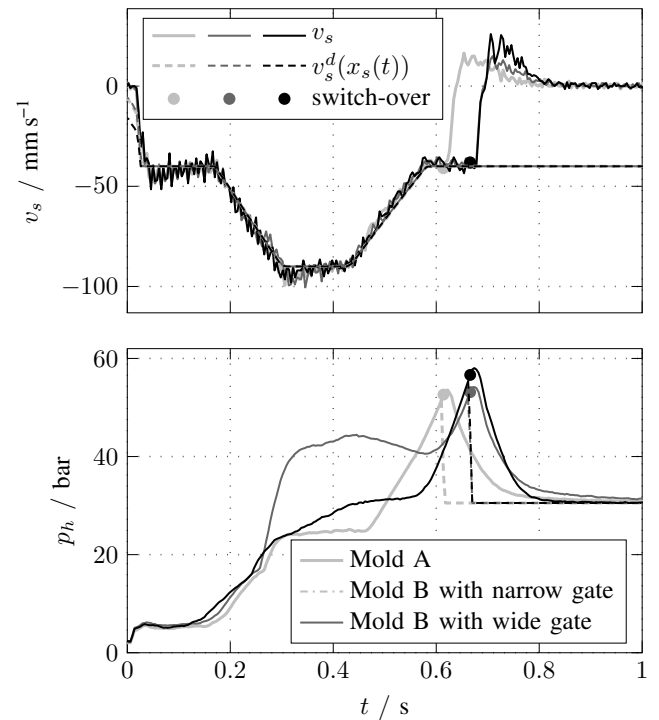


Fig. 11. Measurement results: Form injection experiments into different molds with the MPC.

2) *Melt Cushion Experiment*: While the control performance in the velocity-controlled phase is validated with form injection experiments, the pressure-controlled phase cannot be well investigated with such type of experiments. Therefore, the nozzle is manually closed and the polymer in the antechamber is compressed without possible influences of the mold (melt cushion experiment). An important parameter of this test is the injection stroke, i.e., the volume of the compressed polymer defining the stiffness of the melt cushion. In Fig. 12, the MPC and the state-of-the-art (SOA) controller are compared for an injection stroke of half the screw diameter $D_s/2$, which is a rather stiff melt cushion. At $t = 4.5$ s, the pressure-controlled phase starts and a step-like pressure profile p_h^d is chosen. The MPC shows a slightly better step response behavior in this case resulting in a smaller control error $p_h^d - p_h$ compared to the SOA controller². Both controllers are stationary accurate in the pressure-controlled packing phase. If the same test is performed at a larger injection stroke $2D_s$, i.e., a softer melt cushion, the MPC outperforms the SOA controller as can be seen in Fig. 13. In contrast to the SOA controller the MPC has similar good performance independent of the operating point.

²Note that the control error in the pressure is depicted only after the switch-over point to the pressure-controlled phase.

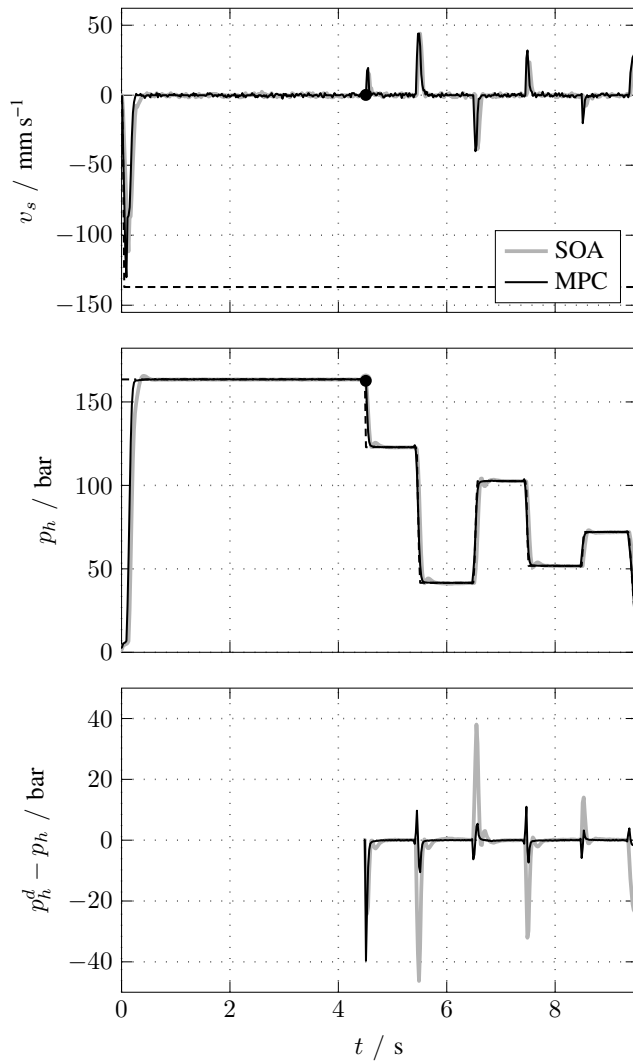


Fig. 12. Measurement results: Melt cushion experiment with injection stroke half the screw diameter $D_s/2$.

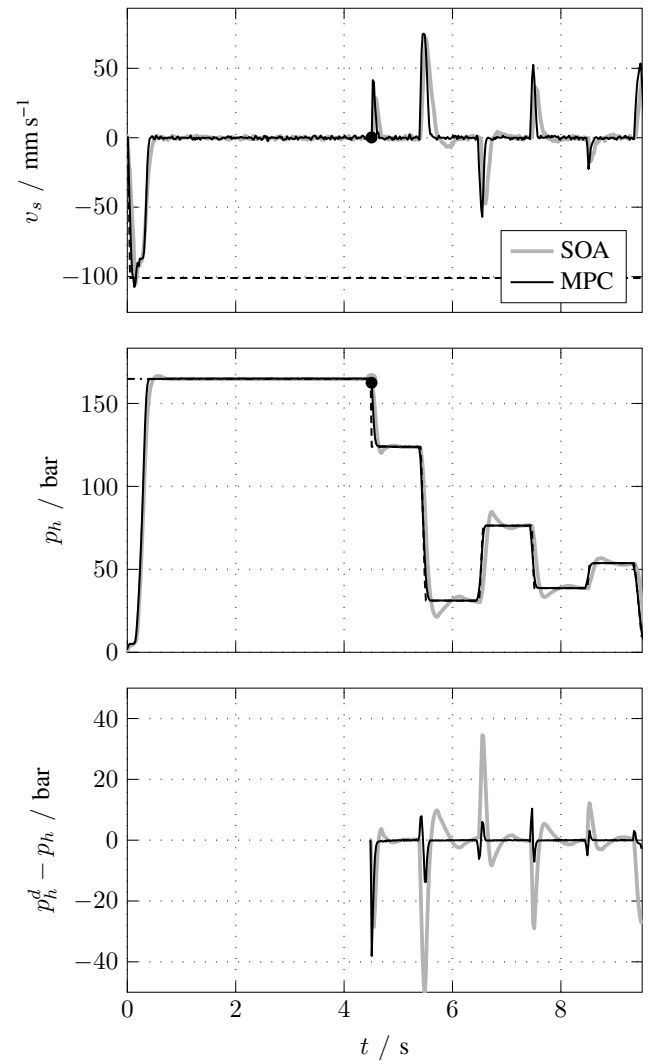


Fig. 13. Measurement results: Melt cushion experiment with injection stroke double of the screw diameter $2D_s$.

C. Sensitivity to Unknown Model-Parameters

A thorough sensitivity analysis of the MPC with respect to varying model parameters was conducted by means of simulation studies. While the geometry parameters of the system are typically well known, the parameters of the hydraulic fluid and the polymer are known only with some uncertainty and even may change over time (aging, entrapped air, etc.). For that reason these parameters of the prediction model were varied and the impact on the controller performance was evaluated. It turned out that the most critical parameters are the bulk moduli of the hydraulic oil β_p , β_{ci} and the polymer β_{ac} as well as the polymer's flow behavior index n . To evaluate the worst-case behavior these parameters were altered simultaneously within their expected range in the real application and the behavior was evaluated by means of a Monte-Carlo simulation. The expected range of the parameters' variation is $\beta_0 = \pm 50\%$ (see (2)), $n = \pm 50\%$ (see (3)), and $\beta_p = \pm 50\%$, $\beta_{ci} = \pm 50\%$ (see (4)). Tab. I and Tab. II summarize the results for the

form injection experiment and the melt cushion experiment, respectively. Here, the nominal case is compared to the worst-case combination of the varied parameters.

TABLE I
MODEL PARAMETER SENSITIVITY: FORM INJECTION.

	$\text{mean} v_s - v_s^d $ mm s^{-1}	$\text{max} v_s < v_s^d $ mm s^{-1}	$\text{max} p_h > p_h^{max} $ bar
nominal	6.2	8.4	3.4
worst-case	26.5	28.4	4.4

The tracking performance for the filling and packing phase is measured by the quantities $\text{mean}|v_s - v_s^d|$ and $\text{mean}|p_h - p_h^d|$. The performance of adhering to the velocity constraint and pressure limit is evaluated by the quantities $\text{max}|v_s < v_s^d|$ and $\text{max}|p_h > p_h^{max}|$. The simulation studies show that the proposed control strategy is able to deal with

TABLE II
MODEL PARAMETER SENSITIVITY: MELT CUSHION TEST.

	mean $ p_h - p_h^d $ bar	max $ v_s < v_s^d $ mm s ⁻¹
nominal	0.4	6.5
worst-case	1.5	7.1

these parameter variations and maintain an acceptable control performance.

V. CONCLUSIONS

In the present work, a model-predictive control strategy for a servo-pump driven injection molding machine was proposed. This strategy systematically considers all the system constraints and is able to handle the velocity-controlled filling and the pressure-controlled packing phase without knowledge of the mold geometry. First, a reduced mathematical model tailored to the needs of the controller design, which covers the essential dynamics and nonlinearities of the injection molding machine, was derived. Since the mold geometry is assumed to be unknown, a Lyapunov-based online-estimator for the volume flow into the mold was developed. Then, the inequality constraints are taken into account in form of penalty functions and the resulting optimal control problem for the MPC is iteratively solved by a computationally efficient Riccati recursion.

The proposed control strategy was implemented with a sampling time of 1 ms on a real-time hardware and a number of experiments were conducted on an industrial injection molding machine. These experiments show that the proposed control strategy significantly improves the control performance compared to the industrial state-of-the-art controllers.

APPENDIX A

LOAD ESTIMATOR WITH TIME-VARYING GAIN

The error system (14) with the time-varying feedback (16b) and (17) is given in the linear time-varying form

$$\frac{d}{dt} \begin{bmatrix} \hat{e}_p \\ \hat{e}_q \end{bmatrix} = \underbrace{\begin{bmatrix} -\lambda_p & \Phi_q \\ -f(v_s)\Phi_q\lambda_q & 0 \end{bmatrix}}_{\mathbf{A}(x_s, v_s, p_h)} \underbrace{\begin{bmatrix} \hat{e}_p \\ \hat{e}_q \end{bmatrix}}_{\hat{\mathbf{x}}_e}. \quad (37)$$

To analyze the stability of the equilibrium $\hat{\mathbf{x}}_e = \mathbf{0}$ the Lyapunov function candidate

$$W_e = \hat{\mathbf{x}}_e^T \mathbf{G} \hat{\mathbf{x}}_e > 0 \quad (38a)$$

is utilized with the positive definite matrix

$$\mathbf{G} = \begin{bmatrix} \frac{\alpha_1}{2\lambda_p} & -\alpha_2 \\ -\alpha_2 & \frac{\alpha_3}{\lambda_q} \end{bmatrix} > 0 \quad (38b)$$

and suitable positive constants α_1 , α_2 , and α_3 . The derivative of (38a) along the trajectories of (37) is given by

$$\frac{d}{dt} W_e = \hat{\mathbf{x}}_e^T (\mathbf{G}\mathbf{A} + \mathbf{A}^T\mathbf{G})\hat{\mathbf{x}}_e = -\hat{\mathbf{x}}_e^T \mathbf{H}\hat{\mathbf{x}}_e < 0. \quad (39)$$

Although \mathbf{H} depends on the operating point (x_s, v_s, p_h) , it can be shown that there exists a set of coefficients α_1 , α_2 , and α_3

such that $\mathbf{G} > 0$ and $\mathbf{H} > 0$ holds true for the whole relevant operating range. Thus, asymptotic stability of (14) with (16b), (17) is proven.

APPENDIX B

ITERATIVE RICCATI RECURSION SCHEME

The QP (36) is solved by a Riccati recursion scheme, which is briefly summarized in the following. The reader is referred to [43], [44], [45] for a more detailed discussion on this method.

At each sampling instant k of the MPC with sampling time T_s , the following steps are performed:

0) Initialization

Calculation of the linearized system Φ_k, Γ_k in the first iteration, i.e., $l = 1$, with the measured (predicted) state $\hat{\mathbf{x}}_{k+N_{td}}$ as discussed in Sec. III-C. To improve robustness, it can be ensured that the eigenvalues of the closed-loop system are located within a circle with radius $0 \leq r \leq 1$ by scaling the linearized system

$$\bar{\Phi}_k = \frac{1}{r} \Phi_k \\ \bar{\Gamma}_k = \frac{1}{r} \Gamma_k.$$

1) Forward integration

In the first iteration, the system (30) is integrated with the optimal solution $\tau_{el,j|k-1}^*$, $j = 0, \dots, N-1$ of the last MPC step $k-1$.

2) Backward recursion

Initialization of $\mathbf{P}_N = \Omega_{N|k}^l$ and $\mathbf{p}_N = \mathbf{g}_{N|k}^l$
for $j = N-1, \dots, 0$ **do**

Calculation of

$$\Omega_{j|k}^l, \left(\mathbf{b}_{j|k}^l\right)^T, \left(\mathbf{g}_{j|k}^l\right)^T, \mathbf{c}_{j+1|k}^l, R_{j|k}^l, d_{j|k}^l$$

from (36)

Update of

$$\mathbf{h}^T = \left(\mathbf{b}_{j|k}^l\right)^T + \bar{\Gamma}_k^T \mathbf{P}_{j+1} \bar{\Phi}_k \\ g = \left(R_{j|k}^l + \bar{\Gamma}_k^T \mathbf{P}_{j+1} \bar{\Gamma}_k\right)^{-1} \\ q = d_{j|k}^l + \bar{\Gamma}_k^T \left(\mathbf{p}_{j+1} - \mathbf{P}_{j+1} \mathbf{c}_{j+1|k}^l\right)$$

$$\mathbf{p}_j = \mathbf{g}_{j|k}^l + \bar{\Phi}_k^T \left(\mathbf{p}_{j+1} - \mathbf{P}_{j+1} \mathbf{c}_{j+1|k}^l\right) - gq\mathbf{h}$$

$$\mathbf{P}_j = \Omega_{j|k}^l + \bar{\Phi}_k^T \mathbf{P}_{j+1} \bar{\Phi}_k - g\mathbf{h}\mathbf{h}^T$$

Store the variables $\mathbf{k}_j = g\mathbf{h}$, $k_j = gq$, $\mathbf{c}_{j+1|k}^l$

end for

3) Forward recursion

Initialize with $\Delta s_{0,k}^l = \mathbf{0}$

for $j = 0, \dots, N-1$ **do**

Linear stabilizing feedback law

$$\Delta \tau_{el,j|k}^l = -\mathbf{k}_j^T \Delta \mathbf{s}_{j|k}^l - k_j$$

Forward integration of the state variables

$$\Delta \mathbf{s}_{j+1|k}^l = -\mathbf{c}_{j+1|k}^l + \Phi_k \Delta \mathbf{s}_{j|k}^l + \Gamma_k \Delta \tau_{el,j|k}^l$$

end for

4) Update of the control inputs and state variables

$$\begin{aligned} \tau_{el,j|k}^{l+1} &= \tau_{el,j|k}^l + \Delta \tau_{el,j|k}^l, \quad j = 0, \dots, N-1 \\ \mathbf{s}_{j|k}^{l+1} &= \mathbf{s}_{j|k}^l + \Delta \mathbf{s}_{j|k}^l, \quad j = 1, \dots, N \end{aligned}$$

5) Check termination criteria

if $\max_{j=0, \dots, N-1} |\Delta \tau_{el,j|k}^l| > \Delta \tau_{el}^{max}$ and $l \leq N_{it}$
then

$l \leftarrow l + 1$

Goto step 2

end if

In addition to the maximum number N_{it} of iterations the maximum change of any input variable $\Delta \tau_{el}^{max}$ is introduced to stop the iteration if the solution is close to the optimum.

APPENDIX C

PARAMETERS OF THE CONTROL STRATEGY

Table III and IV list the values of the parameters of the estimator and MPC, respectively. Here, p_{ref} , n_{ref} , x_{ref} , and v_{ref} are typical values of the specific injection unit.

TABLE III
PARAMETERS FOR THE ESTIMATOR.

Variable	Value	Unit
λ_p	1000	s^{-1}
$\frac{\lambda_q}{(q_{ref}/p_{ref})^2}$	1400	-
$v_{s,q1}/v_{ref}$	0.2	-
f_{min}	0.1	-

TABLE IV
PARAMETERS FOR THE MPC.

Variable	Value	Unit
T_s	1	ms
N_p	10	-
N	6	-
N_{td}	3	-
$Q_{x_s} x_{ref}^2$	0.1	-
$Q_{p_{h,j}} p_{ref}^2, j < N$	20	-
$Q_{p_{h,N}} p_{ref}^2 / N$	20	-
$R_{\tau_{el}} (\tau_{el}^{max})^2$	0.15	-
$\Gamma_{p_h} p_{ref}$	20	-
$\Gamma_{n_p} n_{ref}^2$	100	-
$\Gamma_{\tau_{el}} (\tau_{el}^{max})^2$	1×10^5	-
$\Gamma_{\hat{n}_p} \hat{n}_{ref}^2$	20	-
$\Gamma_{v_{s,j}} v_{ref}^2, j \leq 3$	100	-
$\Gamma_{v_{s,j}} v_{ref}^2, j > 3$	0	-
r	0.95	-
e_s^{max} / D_s	0.3	-
\hat{N}_{it}	10	-
$\Delta \tau_{el}^{max} / \tau_{el}^{max}$	0.4	%

REFERENCES

- [1] C. Froehlich, W. Kemmetmüller, and A. Kugi, "Control-oriented modeling of servo-pump driven injection molding machines in the filling and packing phase (published online, doi: 10.1080/13873954.2018.1481870)," *Mathematical and Computer Modelling of Dynamical Systems*, 2018.
- [2] T. A. Osswald, L.-S. Turng, and P. Gramann, *Injection Molding Handbook*. Munich, Germany: Carl Hanser Verlag, 2008.
- [3] D. V. Rosato, D. V. Rosato, and M. G. Rosato, *Injection molding handbook*. New York, USA: Springer, 2000.
- [4] A. R. Agrawal, I. O. Pandelidis, and M. Pecht, "Injection-molding process control—a review," *Polymer Engineering and Science*, vol. 27, no. 18, pp. 1345–1357, 1987.
- [5] D. Abu Fara, M. R. Kamal, and W. I. Patterson, "Evaluation of simple dynamic models and controllers for hydraulic and nozzle pressure in injection molding," *Polymer Engineering & Science*, vol. 25, no. 11, pp. 714–723, 1985.
- [6] M. R. Kamal, W. I. Patterson, N. Conley, D. Abu Fara, and G. Lohfink, "Dynamics and control of pressure in the injection molding of thermoplastics," *Polymer Engineering and Science*, vol. 27, no. 18, pp. 1403–1410, 1987.
- [7] I. O. Pandelidis and A. R. Agrawal, "Optimal anticipatory control of ram velocity in injection molding," *Polymer Engineering and Science*, vol. 28, no. 3, pp. 147–156, 1988.
- [8] C. M. Dong and A. A. Tseng, "A multivariable self-tuning controller for injection molding machines," *Computers in Industry*, vol. 13, no. 2, pp. 107–122, 1989.
- [9] S. M. Smud, D. O. Harper, P. B. Deshpande, and K. W. Leffew, "Advanced process control for injection molding," *Polymer Engineering and Science*, vol. 31, no. 15, pp. 1081–1085, 1991.
- [10] R. Zhang and F. Gao, "Improved infinite horizon LQ tracking control for injection molding process against partial actuator failures," *Computers and Chemical Engineering*, vol. 80, pp. 130–139, 2015.
- [11] M. A. C. Finn, J. M. Hernández, and R. Dubay, "Cavity peak pressure control during packing using model predictive control theory," in *Proc. of ANTEC 2011, Newton, USA*, vol. 3, 2011, pp. 2408–2412.
- [12] B. Pramujati, R. Dubay, and J. G. Han, "Injection velocity control in plastic injection molding," in *Proc. of ANTEC 2005, Boston, USA*, vol. 2, 2005, pp. 305–309.
- [13] S. Huang, K. K. Tan, and T. H. Lee, "Predictive control of ram velocity in injection molding," *Polymer-Plastics Technology and Engineering*, vol. 38, no. 2, pp. 285–303, 1999.
- [14] Y. Yang and F. Gao, "Adaptive control of the filling velocity of thermoplastics injection molding," *Control Engineering Practice*, vol. 8, no. 11, pp. 1285–1296, 2000.
- [15] M. Abu-Ayyad and R. Dubay, "Development of an extended predictive controller for injection speed," in *Proc. of ANTEC 2007, Ohio, USA*, vol. 2, 2007, pp. 680–683.
- [16] R. Dubay, B. Pramujati, J. Han, and F. Strohmaier, "An investigation on the application of predictive control for controlling screw position and velocity on an injection molding machine," *Polymer Engineering and Science*, vol. 47, no. 4, pp. 390–399, 2007.
- [17] M. Abu-Ayyad, R. Dubay, and J. M. Hernandez, "A nonlinear model-based predictive controller for injection speed," in *Proc. of ANTEC 2009, Illinois, USA*, vol. 5, 2009, pp. 2923–2929.
- [18] J. H. Yang, "Nonlinear adaptive control for injection molding machines," in *Proc. of IECON*, vol. 2, 2002, pp. 1663–1668.
- [19] K. K. Tan, S. N. Huang, and X. Jiang, "Adaptive control of ram velocity for the injection molding machine," *IEEE Transactions on Control Systems Technology*, vol. 9, no. 4, pp. 663–671, 2001.
- [20] H. Daxberger, K. Rieger, and K. Schlacher, "On modelling and control of compressible non-Newtonian injection processes," in *Computer Aided Systems Theory – EUROCAST 2011*, ser. Lecture Notes in Computer Science. Berlin, Germany: Springer, 2012, vol. 6928, pp. 65–72.
- [21] S.-O. Lindert, G. Reindl, and K. Schlacher, "Identification and control of an injection moulding machine," in *Proc. of the 19th IFAC World Congress*, vol. 47, no. 3, Cape Town, South Africa, 2014, pp. 5878–5883.
- [22] H.-P. Tsoi and F. Gao, "Control of injection velocity using a fuzzy logic rule-based controller for thermoplastics injection molding," *Polymer Engineering and Science*, vol. 39, no. 1, pp. 3–17, 1999.
- [23] S. Wang, J. Ying, Z. Chen, and K. Cai, "Grey fuzzy PI control for packing pressure during injection molding process," *Journal of Mechanical Science and Technology*, vol. 25, no. 4, pp. 1061–1068, 2011.

- [24] J. Lin and R. J. Lian, "Self-organizing fuzzy controller for injection molding machines," *Journal of Process Control*, vol. 20, no. 5, pp. 585–595, 2010.
- [25] G. Ouyang, X. Li, X. Guan, Z. Zhang, X. Zhang, and R. Du, "Ram velocity control in plastic injection molding machines with neural network learning control," in *Advances in Neural Networks*, ser. Lecture Notes in Computer Science. Berlin, Heidelberg: Springer, 2004, vol. 3174, pp. 169–174.
- [26] S. N. Huang, K. K. Tan, and T. H. Lee, "Neural-network-based predictive learning control of ram velocity in injection molding," *IEEE Transactions on Systems, Man, and Cybernetics, Part C: Applications and Reviews*, vol. 34, no. 3, pp. 363–368, 2004.
- [27] H. Havlicsek and A. Alleyne, "Nonlinear control of an electrohydraulic injection molding machine via iterative adaptive learning," *IEEE/ASME Transactions on Mechatronics*, vol. 4, no. 3, pp. 312–323, 1999.
- [28] F. Gao, Y. Yang, and C. Shao, "Robust iterative learning control with applications to injection molding process," *Chemical Engineering Science*, vol. 56, no. 24, pp. 7025–7034, 2001.
- [29] K. K. Tan and J. C. Tang, "Learning-enhanced PI control of ram velocity in injection molding machines," *Engineering Applications of Artificial Intelligence*, vol. 15, no. 1, pp. 65–72, 2002.
- [30] D. Zheng and A. Alleyne, "Modeling and control of an electro-hydraulic injection molding machine with smoothed fill-to-pack transition," *Journal of Manufacturing Science and Engineering*, vol. 125, no. 1, pp. 154–163, 2003.
- [31] J. Shi, F. Gao, and T.-J. Wu, "Robust iterative learning control design for batch processes with uncertain perturbations and initialization," *AICHE Journal*, vol. 52, no. 6, pp. 2171–2187, 2006.
- [32] Z. Cao, Y. Yang, J. Lu, and F. Gao, "Two-time-dimensional model predictive control of weld line positioning in bi-injection molding," *Industrial & Engineering Chemistry Research*, vol. 54, no. 17, pp. 4795–4804, 2015.
- [33] D. Dörner, T. Radermacher, B. Wagner, and J. Weber, "Iterative learning control of a plastics injection molding machine," (in German), at - *Automatisierungstechnik*, vol. 62, pp. 226–236, 2014.
- [34] S.-J. Huang and T.-H. Lee, "Application of neural networks in injection moulding process control," *The International Journal of Advanced Manufacturing Technology*, vol. 21, no. 12, pp. 956–964, 2003.
- [35] Y.-g. Peng, J. Wang, and W. Wei, "Model predictive control of servo motor driven constant pump hydraulic system in injection molding process based on neurodynamic optimization," *Journal of Zhejiang University Science C*, vol. 15, no. 2, pp. 139–146, 2014.
- [36] M. Reiter, S. Stemmler, C. Hopmann, A. Reßmann, and D. Abel, "Model predictive control of cavity pressure in an injection moulding process," in *Proc. of the 19th IFAC World Congress*, vol. 47, no. 3, Cape Town, South Africa, 2014, pp. 4358–4363.
- [37] P. Kennedy and R. Zheng, *Flow Analysis of Injection Molds*. Munich, Germany: Carl Hanser Verlag, 2013.
- [38] W. Kemmetmüller, F. Fuchshumer, and A. Kugi, "Nonlinear pressure control of self-supplied variable displacement axial piston pumps," *Control Engineering Practice*, vol. 18, no. 1, pp. 84–93, 2010.
- [39] P. Kokotović, H. Khalil, and J. O'Reilly, *Singular Perturbation Methods in Control: Analysis and Design*. Society for Industrial and Applied Mathematics, 1999.
- [40] H. K. Khalil, *Nonlinear Systems*. Upper Saddle River, USA: Prentice Hall, 2002.
- [41] T. Geyer, *Model Predictive Control of High Power Converters and Industrial Drives*. Chichester, United Kingdom: John Wiley & Sons Inc, 2016.
- [42] E. F. Camacho and C. Bordons, *Model Predictive control*. London, UK: Springer, 2007.
- [43] M. Diehl, *Real-Time Optimization for Large Scale Nonlinear Processes*. Düsseldorf, Germany: VDI Verlag, 2002.
- [44] M. C. Steinbach, "Fast recursive SQP methods for large-scale optimal control problems," Ph.D. dissertation, Universität Heidelberg, Heidelberg, Germany, 1995.
- [45] C. V. Rao, S. J. Wright, and J. B. Rawlings, "Application of interior-point methods to model predictive control," *Journal of Optimization Theory and Applications*, vol. 99, no. 3, pp. 723–757, 1998.



Christoph Froehlich (S'10) received the M.Sc. degree in automation technology from TU Wien, Vienna, Austria, in 2015.

Since 2015 he is a Research Assistant with the Automation and Control Institute (ACIN), TU Wien, Vienna, Austria. His research activities are within the fields of mathematical modeling, identification and control of nonlinear dynamical systems with applications in the steel industry as well as the polymer processing industry.



Wolfgang Kemmetmüller (M'04) received the Dipl.-Ing. degree in mechatronics from Johannes Kepler University Linz, Linz, Austria, in 2002, the Ph.D. (Dr.Eng.) degree in control engineering from Saarland University, Saarbrücken, Germany, in 2007 and the Habilitation degree in system theory and automatic control from TU Wien in 2016.

He was a Research Assistant with the Chair of System Theory and Automatic Control, Saarland University, from 2002 to 2007. From 2007 to 2012, he was a Senior Researcher with the Automation and Control Institute (ACIN), TU Wien, Vienna, Austria, where he currently is an Associate Professor. His current research interests include the physics-based modeling and the nonlinear (optimal) control of mechatronic systems, where he is involved in several industrial research projects. Dr. Kemmetmüller is an Associate Editor of the IFAC journal *Mechatronics* and the journal *Mathematical and Computer Modeling of Dynamical Systems*.



Andreas Kugi (M'94) received the Dipl.-Ing. degree in electrical engineering from TU Graz, Austria, and the Ph.D. degree in control engineering from Johannes Kepler University (JKU), Linz, Austria, in 1992 and 1995, respectively. In 2000, he got the habilitation in the field of control theory and automatic control at JKU and he was a full professor for system theory and automatic control at Saarland University in Germany from 2002 to 2007. Since June 2007, he is a full professor for complex dynamical systems and head of the Automation and Control Institute at

TU Wien, Austria and since 2017, he is also the head of the Center for Vision, Automation & Control at the Austrian Institute of Technology (AIT). His main research interests include the modeling, nonlinear control and optimization of complex dynamical systems, the mechatronic system design, as well as robotics and process automation with a focus on industrial applications. He is full member of the Austrian Academy of Sciences and member of the German National Academy of Science and Engineering (acatech).